International Journal of Mechanical, Industrial and Aerospace Sciences
ISSN: 2517-9950
Vol:3, No:10, 2009

Engine Power Effects on Support Interference

B.J.C. Horsten and L.L.M. Veldhuis

Abstract—Renewed interest in propeller propulsion on aircraft configurations combined with higher propeller loads lead to the question how the effects of the propulsion on model support disturbances should be accounted for. In this paper, the determination of engine power effects on support interference of sting-mounted models is demonstrated by a measurement on a four-engine turboprop aircraft. CFD results on a more generic model are presented in order to clarify the possible mechanism behind engine power effects on support interference. The engine slipstream induces a local change in angle of sideslip at the model sting thereby influencing the sting near-field and far-field effects. Whether or not the net result of these changes in the disturbance pattern leads to a significant engine power effect depends on the configuration of the wind tunnel model and the test setup.

Keywords—CFD, engine power effects, measurements, support interference.

I. Introduction

When the problem of model support interference is addressed, an accurate description of the disturbances of interest is necessary. Generally speaking, model support disturbances can be defined as "... all the disturbances in the model flowfield induced by the presence of its supporting parts ...". The manifestation of the disturbances of the model support on the flowfield of interest (being a volume containing the wind tunnel model) can be divided in two main classes (Horsten et al. [1]):

1) Support near-field effects: Near-field effects consist of viscous and inviscid disturbances manifesting in the direct vicinity of the protrusion of model support and wind tunnel model (on the fuselage of the model). The near-field effects are caused by the support part protruding the fuselage boundary layer (such as a sting or bayonette). Typical effects include a streamline displacement on the model, a carry-over of support pressure distribution onto the model and model boundary layer disturbances caused by the protrusion and presence of the support
2) Support far-field effects: Far-field effects are inviscid disturbances expressed in a buoyancy effect on the wind tunnel model fuselage and inviscid disturbances that influence the local flow properties at the lifting surfaces of the model. Generally speaking, these disturbances manifest in local changes of angle of attack α, angle of sideslip β and dynamic pressure q.

B.J.C. Horsten is a PhD. student at the Department of Aerodynamics at the Faculty of Aerospace Engineering, Delft University of Technology, Kluyverweg 2, 2629 HT, Delft, The Netherlands. Email: B.J.C.Horsten@tudelft.nl
L.L.M. Veldhuis is an associate professor at the Department of Aerodynamics at the Faculty of Aerospace Engineering, Delft University of Technology, Kluyverweg 2, 2629 HT, Delft, The Netherlands. Email: L.L.M.Veldhuis@tudelft.nl
Manuscript received July 1, 2009; revised September 17, 2009.

Of course there are exceptions to these definitions. A model support may contain a part that does not protrude the boundary layer of the model but is close enough to the model surface to carry over its pressure distribution. These type of support setups are however not desirable because they are likely to provide with large disturbances on the model. For that purpose they are not considered in this paper. The support part protruding the model boundary layer will cause both a near-field and a far-field effect on the windtunnel model. It will be clear that the magnitude of the far-field effect is dependent on the magnitude of the near-field effect. Large local disturbances at the protrusion of the support will also disturb the flow at the lifting surfaces. Support parts that do not protrude the model boundary layer only cause far-field effects.

The values of near-field and far-field effects depend on the disturbance potential ϕ of the model support. This potential is influenced by a number of factors:

1) The geometrical characteristics of the support and model
2) The placement of the support relative to the model (Veldhuis [2])
3) Incoming flow conditions

With respect to the first two points; Different wind tunnel model geometries and/or support placements with respect to the model will cause the disturbances of the model support to change. The reason for this is that the value of ϕ changes when the local boundary layer properties at the support protrusion location changes and if the support is connected to the model at locations of pressure gradients of various nature. Adjusting the geometrical characteristics of the support will lead to a change in disturbance potential seen as a local and global increase or decrease of the disturbance. When the inflow conditions of model and support change (velocity magnitude and/or direction) this will have an effect on the support disturbance signature as well. Changing this signature, the near-field and far-field effects will also change in magnitude.

The total disturbance of a certain support configuration (both near-field effects and far-field effects) on one of the aerodynamic coefficients of a wind tunnel model can be given by:

$$\Delta C_i = \Delta C_{i_{primary}} + \Delta C_{i_{secondary}} \quad (1)$$

According to Equation 1, the total disturbance is a composition of a primary and a secondary disturbance. The primary disturbances consist of the summation of near-field and far-field effects of the parts spanning the model support setup in

a wind tunnel at given free-stream conditions causing a certain value of ϕ. Secondary disturbances are *additional* disturbances caused by a change in disturbance potential of the support ($\Delta\phi$ usually locally) and thereby influence the near-field and far-field effects. Examples of secondary disturbances are:

- Wind tunnel wall proximity effects: When during a wind tunnel test the support geometry approaches the wind tunnel walls closely, both the pressure signature on the walls as on the support will change. This leads to a change in disturbance potential of the model support leading to a change in near-field and far-field effects
- Engine power effects: When a wind tunnel model is equipped with one or more engines (propeller or jet), the aerodynamic characteristics of the model will change. The measured lift of the aircraft will increase due to locally higher dynamic pressures. Not only lift-, but also drag- and pitching moment-coefficients (think of the effect of the engine slipstream over the stabilizer) show a strong dependency on engine thrust setting. The adapted streamline pattern around the model configuration (due to the interference of the slipstream) will also affect the aerodynamic characteristics. Besides the fact that the model aerodynamics itself is directly affected by the engine slipstream, the engines also affect the flow around the model support parts. When using external balances, these effects can be directly measured. This is not the case for internal balances. When the flow around the support changes, the interference of the support on the model also changes. This effect is defined as an engine power effect on the support disturbance. The effect of the engine slipstream on the support corrections is translated in a change of interference from the support onto the wind tunnel model. This is measurable because the change in flow field characteristics caused by the changing support disturbance potential ϕ directly affects the model flow field

In this paper, engine power effects on support interference are the subject of interest. In the next sections, these effects are illustrated using results of low-speed (free-stream Mach number $M_\infty \approx 0.20$) wind tunnel measurements on a four-engine turboprop aircraft in the Large Low-Speed Facility (LLF) of the German-Dutch Wind Tunnels (DNW). Based on dummy measurements, the determination of the secondary disturbances is demonstrated along with their nature and order of magnitude. Calculations on engine power effects are also performed. Their setup and results will be discussed. The possible mechanism determining engine power effects on support interference will be discussed. Based on this, recommendations regarding the test setup are given in order to prevent large secondary disturbances in future wind tunnel tests.

II. Measuring Engine Power Effects

One of the ways to find support interference effects is to perform dummy measurements for all configurations under consideration (tail on/off, different wing configurations, varying Mach numbers, angles of attack, sideslip etc.). Measurements with various support configurations are combined to lead to the corrections of force and moment coefficients for the support setup of interest. Examples of such setups are given in Fig. 1.

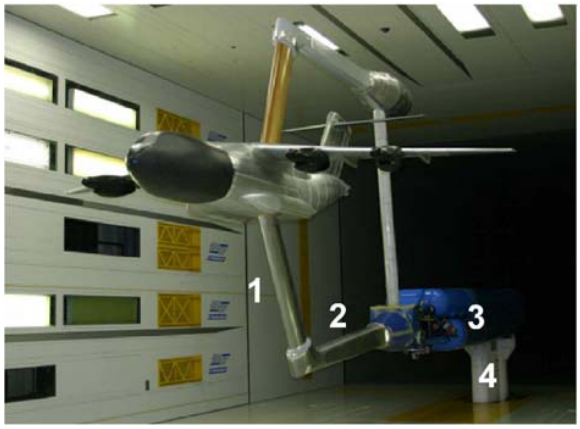

(a)

(b)

Fig. 1. Measurement setup of a low-speed measurement on a four-engine turboprop aircraft in the LLF of DNW showing (a) An example of a dummy dorsal setup. The model is supported by a ventral support while a dummy dorsal setup is installed. The numbers in the figure correspond to the model sting (1), the horizontal sting (2) the torpedo (3) and the sword (4) (b) An example of a dorsal setup

Fig. 1 illustrates examples of a dummy measurement setup and a dorsal setup of a four-engine turboprop aircraft as measured in the LLF of DNW. The ventral and dorsal support structures consists of a model sting (protruding the model surface) that is attached to a horizontal sting. The horizontal sting is attached at the back to a nacelle-like structure called the torpedo. This torpedo connects to the so called sword, a support part that is connected to the tunnel floor. Dorsal- and ventral setups are measured in the tunnel. Their support corrections are of interest. An additional dummy setup simulating the combined dorsal and ventral setup is therefore also measured to determine these primary disturbances. Subtracting for example the measurement results of the dorsal setup (Fig. 1(b)) from the results of the dummy dorsal

measurement setup (Fig. 1(a)), the outcome will indicate the magnitude of the primary support interference of the ventral setup (Eckert [3]).

The key to successively measuring engine power effects is to perform two dummy measurement campaigns, one campaign at "power-on" (engines running) and the other campaign at "power-off" (engines not running) conditions. For both campaigns the dummy measurements are used in order to calculate the support interference by performing linear operations on the dummy measurement data. The difference between the power-on and power-off support corrections indicates the magnitude of engine power effects on support interference. Depending on the configuration of the wind tunnel model an elegant method of categorizing the measured support disturbances (both for power-on and power-off test conditions) proposes a division of the total support correction in four distinctive parts (Eckert et al. [4]):

1) A basic support correction for the wind tunnel model fuselage and wing, no tail (horizontal and vertical tailplane) installed, at a certain angle of attack α and zero sideslip β. This correction forms the base of the support corrections
2) An additional correction for this configuration is carried out when angles of sideslip are introduced
3) When a tail (horizontal and vertical tailplane) is installed on the model, a tail installation correction is added to the base support correction (β = 0°)
4) If the model with tail (horizontal and vertical tailplane) is set at a sideslip angle, a third addition is necessary to include the sideslip disturbances at the tail

This method is elegant because like the model during a wind tunnel test, the corrections are made modular thereby enabling their use for tests of aircraft of the same family (with a high test- and setup comparability). In this paper the first correction (from now on called the "base" correction) and the second correction (referred to as the "basic sideslip" correction) are treated and the engine power effects on these corrections are studied. To this end, both corrections are determined for the power-on and power-off case and compared to each other. The test under consideration concerns a low speed measurement of a four-engine turboprop aircraft in the LLF of DNW. Measurement data of this campaign is used to determine engine power effects on the base- and the basic sideslip correction. This is demonstrated in the next two sections.

A. Engine Power Effects on the Base Correction

For both power-on and power-off conditions dummy measurements are carried out on the configuration consisting of a fuselage and wing, no tail installed, at a certain angle of attack α and zero sideslip β. Consider the power-off case first. Performing linear operations on the dummy measurement data (by subtraction of the measurement results) leads to the values of the total support disturbance on the lift-, drag- and pitching moment-coefficients. These disturbances are converted to the so called "disturbance parameters" by applying the method proposed by Eckert ([3]):

- $\Delta\alpha_w$: The angle of attack disturbance at the wing's three-quarter chord position (a far-field effect). This value is a wing spanwise averaged value and is caused by a combined effect of streamline curvature and lift interference of the support structure
- $\Delta q_w/q$: The disturbance of dynamic pressure at the wing's quarter chord position (a far-field effect). This value is also a wing spanwise averaged value. The disturbance is caused by solid and wake blockage of the support
- C_{NT}: A disturbance in model normal direction that embodies the viscous near-field effects on the fuselage
- C_{TT}: A disturbance in model tangential direction that embodies a combination of the support buoyancy at the model and tangential viscous near-field effects. Both the concentrated loads C_{NT} and C_{TT} act at unknown distances X_T and Z_T from the model aerodynamic center

Converting the disturbances of the power-off dummy campaign to the values of the disturbance parameters leads to no problems. Problems do arise however when this same exercise is carried out for the power-on case. A difficulty with this approach is the successive subtraction of the various measurements before arriving at the disturbances on the coefficients. Because the measurements are performed with slightly alternating thrust levels of the engines the aerodynamic coefficients can not be subtracted. This is caused by the high dependency of the coefficients on the thrust level of the engines. This implies that when longitudinal coefficients from two measurements are subtracted, the coefficients will have to be adjusted such that the thrust level of the measurements is equal. It could be decided to make all the measurements "thrust free", meaning that all the longitudinal coefficients are reduced to a thrust level of zero. This however would imply very high corrections (in the order of the value of the measured coefficients) especially at large negative and positive angles of attack. Because during this campaign results of a dorsal- and ventral measurement are subtracted from the results of a dummy measurement setup to arrive at the ventral and dorsal support corrections respectively, it is chosen to keep the dummy measurement setup as a reference. This implies that the longitudinal coefficients of the dorsal- and ventral measurements are adjusted to the thrust level of the dummy measurement at every angle of attack. This "coefficient reduction" can be performed in two different ways:

1) Using a semi-theoretically, semi-empirically determined value of $\frac{\mathrm{d}C_l}{\mathrm{d}C_T}$ where C_T is the configuration thrust coefficient. The theory (Eckert et al. [4]) is based on the principles of super-velocity caused by a propeller in front of the wing. It is assumed that the lift of the wing is build up of a clean, no thrust value of the lift (that is representative for the actual circulation of the wing that can be used to correct for the lift interference in the wall corrections) and an additional lift term that is caused by super-velocity. The corrections on the drag- and the

pitching moment-coefficients are based on this super-lift as well. The constants appearing in the formulas are determined using experimental data

2) Using experimental data to construct various cross plots in order to determine the value of $\frac{dC_i}{dC_T}$. Because two power settings are measured in the campaign under consideration (a low and a moderate power setting), a linear relation is deduced

Both methods are applied and compared. The corrections they propose are of the same nature and order of magnitude. Measurements with more than two power settings might clarify whether or not the value of $\frac{dC_i}{dC_T}$ can indeed be considered linear. This indicates one of the great disadvantages of the second method: Because standard interpolation techniques are used, two or more power settings have to be measured.

Here, the method proposed by Eckert et al. ([4]) is used to set the measurement results to the same thrust level as found for the dummy setup for every angle of attack. Reduction of lift-, drag- and moment-coefficients of the ventral and dorsal measurements to a reference base (subscript B) is performed using the following equations:

$$
\begin{aligned}
C_{L,C_{T_B}} &= C_{L,C_T} \frac{F\left(C_{T_B}\right)}{F\left(C_T\right)} \\
C_{D,C_{T_B}} &= C_{D,C_T} + \frac{C_{L,C_T}^2}{\pi \Lambda} \left(\left(\frac{F\left(C_{T_B}\right)}{F\left(C_T\right)} \right)^2 - 1 \right) \\
C_{M,C_{T_B}} &= \left(C_{M,C_T} - C_{M,C_{T_0}} \right) \frac{F\left(C_{T_B}\right) - 1}{F\left(C_T\right) - 1} + C_{M,C_{T_0}} \\
F\left(C_T\right) &= 1 + k \frac{D_p}{b} \sum_{i=1}^{n} \frac{c_i}{\overline{c}} \left(\sqrt{\frac{\sqrt{1 + C_{T_i}} + 1}{2\sqrt{1 + C_{T_i}}}} \right) C_{T_i}
\end{aligned}
\tag{2}
$$

In Equation set 2, Λ stands for the aspect ratio of the wing, k is a shape factor to compensate the formulas for the absence of the modeling of propeller swirl effects changing the local angle of attack at the wing and a nacelle volume underneath the wing, D_p is the propeller diameter, b is the wing span, $\overline{c}$ the mean aerodynamic chord and c_i the local chord at the wing part wetted by the slipstream of propeller i. For the reduction of the drag-coefficient it is assumed that the viscous component of drag does not need a thrust reduction and that reduction of the induced drag will cover most of the correction. Reductions of both methods are applied to the dorsal and ventral measurements (with respect to the dummy measurement base with a moderate power setting). The reductions can be compared for various flap settings. This comparison is visualized for the ventral setup in Fig. 2.

In Fig. 2 it is seen that both methods provide with similar reductions on the longitudinal coefficients except for the cases where the flaps are deflected at high values (landing configuration). Reasons for this might be that at these flap settings, a linear reduction of the coefficients is not accurate anymore. Also in the method by Eckert, a contraction of the jet over the wing and a deformation of the slipstream caused by

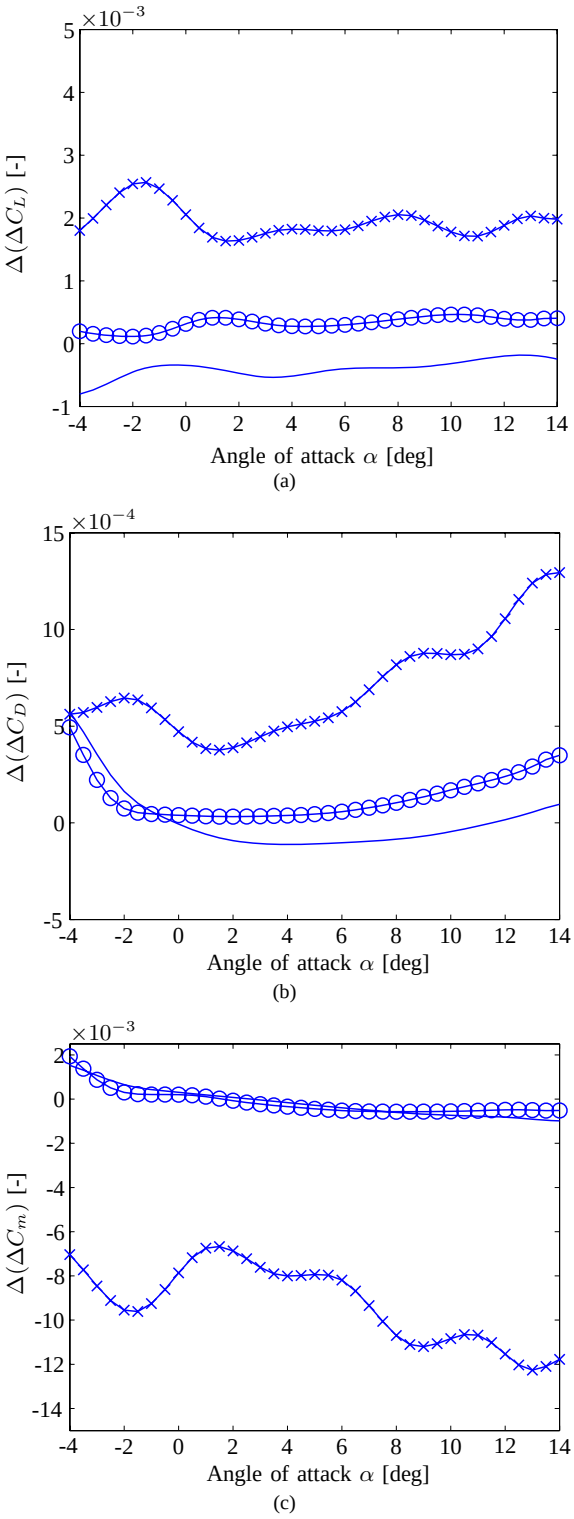

Fig. 2. Trends of the differences of corrections of longitudinal coefficients for thrust level variations between the method as proposed by Eckert et al. ([4]) and a linear reduction method for the (a) Lift-coefficient (b) Drag-coefficient (c) Pitching moment-coefficient for a four-engine turboprop low speed power-on test in the LLF of DNW at moderate power setting. In the plots various flap deflections are shown (– = cruise, o = take-off and x = landing) for the ventral setup

the wing are not taken into account. Because the shape factor k is found as a "best mean" value based on measurements it is possible that this value does not match the high flap settings.

When these reductions are applied to the dorsal and ventral measurements, leveling these to the same thrust setting as the dummy measurements, linear operations are carried out on the measurements to arrive at the support corrections. These corrections are converted to the values of the disturbance parameters as given in [3]. The values of these parameters can be compared to the values in the case a power-off test is performed. This leads to the order of magnitude and nature of the engine power effects. These effects are seen in Fig. 3 for the ventral setup with a moderate power setting.

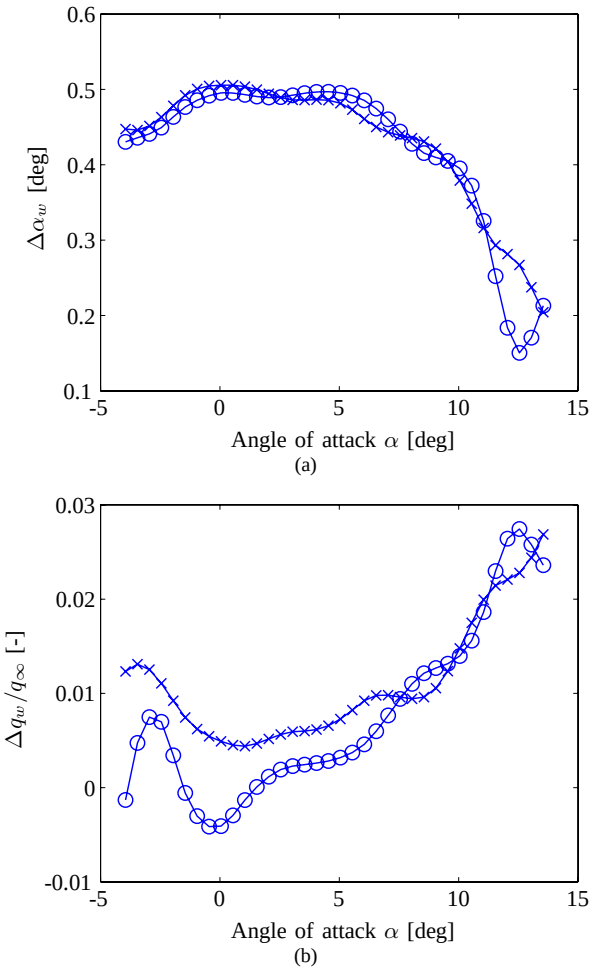

Fig. 3. Engine power effects on the values of (a) $\Delta\alpha_w$ (b) $\frac{\Delta q_w}{q_\infty}$ for the ventral setup of a low-speed measurement on a four-engine turboprop aircraft in the LLF of DNW. Comparison of disturbance parameters between power-off (o) and power-on (x) conditions with a moderate power setting

As can be seen in Fig. 3, a change in disturbance potential of the model support due to the slipstream of the propellers is noticeable. The difference between the power-on and power-off disturbance parameters indicates the order of magnitude of the effect. It is seen that the trends of the support interference with angle of attack do not change. The magnitude of the power-effect is overall moderate compared to the absolute value of the disturbance. These effects are however not negligible.

B. Engine Power Effects on the Basic Sideslip Correction

Besides engine power effects on the base correction, the other corrections are also influenced by the engine slipstream. A good example is the basic sideslip correction. This is an additional correction accounting for the fuselage-wing configuration at angles of sideslip. The magnitude of the engine power effects on these corrections is calculated by comparing the values of the corrections on the aerodynamic force- and moment coefficients between power-on and power-off conditions. For the power-on condition prior to subtraction of the measurement results of the various support setups, the results of the ventral and dorsal measurements have to be elevated to the same power setting as the dummy measurement. Typical results of engine power effects on the lift- and drag correction of a ventral setup with a take-off flap setting at a moderate thrust level are shown in Fig. 4.

When compared to the values of the power-off basic sideslip correction, it seems that both power-off correction as engine power effect are of the same order of magnitude. The power effects are worth including in the correction process.

Besides being able to calculate the values of engine power effects on support interference from dummy measurements, understanding the possible mechanism that leads to these effects is of crucial importance for avoiding future situations where high undesirable power effects arise. To this purpose, CFD calculations are performed. The setup of these calculations and implementation of their results is discussed in the next section.

III. CFD Calculations on Engine Power Effects

Once again referring to Fig. 1 it is seen that the support part that will be mostly affected by a change in disturbance potential ($\Delta\phi$) due to engine power effects is the vertical model sting. Assuming that the interaction of the slipstream of the engines with the remaining support structure is negligible the model sting becomes the support part of interest. For CFD purposes this implies that not the complete support structure should be modeled reducing the amount of computational expenses considerably.

In order to assess engine power effects at one free-stream condition (meaning one angle of attack, angle of sideslip, Mach number) and at one configuration setting (for instance one engine power setting and flap setting), 4 calculations are performed. These calculations are:

1) One calculation modeling the wind tunnel, aircraft fuselage and wing, rotating propellers and model sting

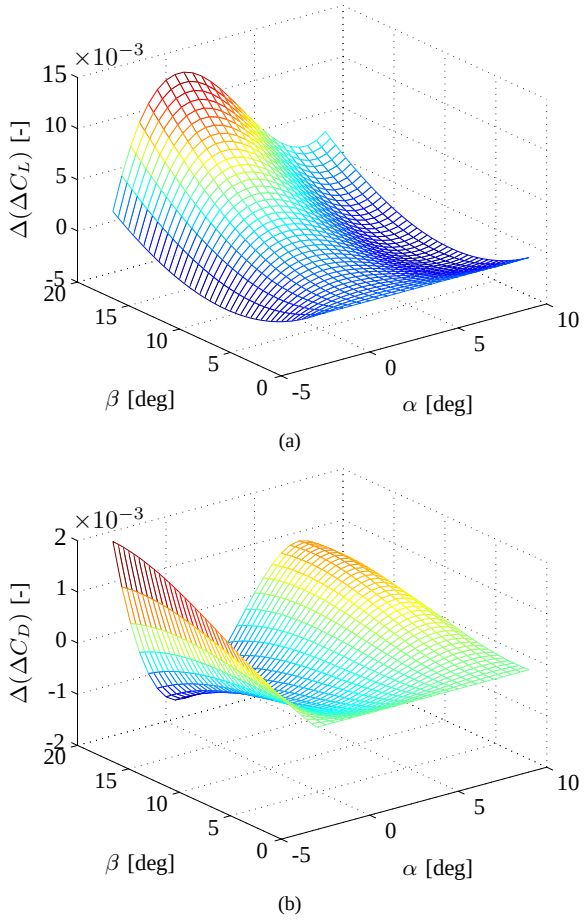

Fig. 4. Engine power effects on the basic sideslip correction. Effects on the values of the (a) Lift correction and (b) Drag correction for the ventral setup of a low-speed measurement on a four-engine turboprop aircraft in the LLF of DNW with a take-off flap setting at a moderate thrust level

2) One calculation modeling the wind tunnel, aircraft fuselage and wing and rotating propellers
3) One calculation modeling the wind tunnel, aircraft fuselage and wing and model sting
4) One calculation modeling the wind tunnel, aircraft fuselage and wing

After every calculation, the forces and moments on the aircraft configuration are determined. Subtracting these results from the first two calculations leads to the support interference effects in power-on conditions. Subtracting the results of the third and fourth calculations leads to the support interference effects in power-off conditions. Finally subtracting the power-off from the power-on interference effects leads to the values of the engine power effects on the support interference.

The computational domain of the calculations performed are based on the wind tunnel tests on model support interference presented in [1]. The bounds of the computational domain coincide with the test section walls where inlet and outlet planes are extended upstream and downstream respectively such as to guarantee the integrity of the inlet and outflow boundary conditions. The aircraft fuselage and sting as the position of the sting with respect to the fuselage are the same as presented in [1]. Unlike the experiment according to Horsten et al. ([1]), the model sting is attached to the fuselage instead of inserted into the fuselage. Internal balance cavity and slit separating the model sting and fuselage are not modeled. When the near-field effect of the model sting is studied, this would be sensible as indicated in [1]. It is expected however that modeling the slit and internal cavity have no distinct influence on the *change* of disturbance potential due to the engine slipstream. The wing that is modeled is a straight wing without taper, sweep and dihedral with a $NACA64_2(A)015$ profile. Modeling of the wing is necessary because the wing has a distinct influence on the slipstream properties of the engines. A deformed slipstream is likely to induce a different value of $\Delta\phi$ at the model sting. Two co-rotating propellers are modeled in front of the wing. Their dimensions, placement and thrust properties are typical for modern turboprop aircraft. A picture of the aircraft configuration including model sting and propellers is given in Fig. 5. Geometrical characteristics of the setup are given in Table I.

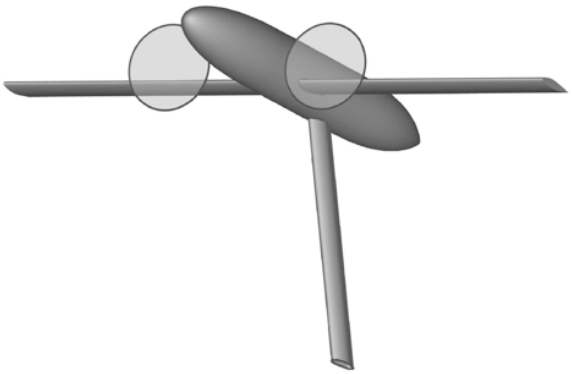

Fig. 5. A graphical representation of the aircraft configuration used to calculate engine power effects on support interference. Fuselage, wings, propeller planes and model sting are clearly discernible

Besides the configuration as shown in Fig. 5, another configuration is generated excluding the model sting. Because the propeller planes are modeled as actuator discs, changing the boundary conditions of these discs leads to the distinction between a power-on and a power-off case. This leads to four distinct cases mentioned earlier in this section to calculate engine power effects on support interference.

It is thought that solving for the unsteady Euler equations will provide with sufficient information on engine power

TABLE I
GEOMETRICAL PROPERTIES OF THE NUMERICAL DOMAIN FOR CALCULATING ENGINE POWER EFFECTS ON SUPPORT INTERFERENCE

Parameter	Value
Test Section Dimensions [W X H]	1.80 X 1.25 [m]
Fuselage Length	1.35 [m]
Fuselage Maximum Thickness	0.16 [m]
Wing Span	1.45 [m]
Wing Mean Aerodynamic Chord	0.15 [m]
Wing Taper Ratio	1.0
Wing Sweep	0.0 [deg]
Wing Dihedral	0.0 [deg]
Sting Chord	0.091 [m]
Propeller Diameter	0.21 [m]

effects. To this end, inviscid meshes (no boundary layers are discretized) are generated consisting of triangular cells. The unsteady Euler equations are solved on these meshes using a second order discretization. The settings characterizing the flow properties and propeller action are given in Table II.

TABLE II
SETTINGS CHARACTERIZING THE FLOW PROPERTIES AND PROPELLER ACTION FOR DETERMINING ENGINE POWER EFFECTS ON SUPPORT INTERFERENCE

Parameter	Value
Medium Characterization	Incompressible Ideal Gas
Angle of Attack α_∞	0 [deg]
Angle of Sideslip β_∞	0 [deg]
Mach Number M_∞	0.147
Thrust Coefficient C_T	0.29
Advance Ratio J	0.94

As seen in Table II it is chosen to select a high power setting in order to create a "worst case scenario". The thrust of the propeller discs is realized by prescribing a pressure jump over the actuator discs. The propeller swirl is prescribed such as to vary over the actuator disc from the hub to the tip with $\frac{1}{r}$ where r is the local radius of the disc having a value of 0 at the hub. The strength of the swirl is calculated according to the swirl model proposed in [5].

The unsteady calculations are solved to improve the rate of iteration convergence. The converged solutions are used in order to analyze the magnitude and nature of the engine power effects. This is presented in the next section.

A. CFD Results on Engine Power Effects

Performing linear operations on the values of lift-, drag- and sideforce-coefficients of the fuselage provides with the power-on and power-off support near-field corrections. Subtracting these values leads to the value of the power effects on near-field support interference. It is found that the engine power effects on the values of the near-field lift-, drag- and sideforce interference is negligible for the current configuration. The order of the power effects is close to typical balance accuracy. The largest effect is on the value of the interference on the fuselage sideforce (order of magnitude = 3 Counts where 1 Count represents a distinguishable 0.001 in the sideforce coefficient). The same exercise can be performed for lift- and drag-coefficients of the wings. The result indicates the power effects on the far-field support interference. Once again it is found that the order of magnitude is negligible.

Because the power effects on the near-field and far-field support disturbances are net (integrated) results it is wise to postpone judgment on these effects and first take a closer look at the engine power effects on the disturbances locally. It is possible that locally the near-field and far-field disturbances are affected to quite some extend. If these local effects (on e.g. the fuselage or the wings) cancel out due to the configuration studied, the net result will not reveal the true nature of the power effects on support interference.

Due to the slipstream drift of the co-rotating propellers the streamlines in front of the model support are given an induced angle of sideslip. The magnitude of this induced angle is of the order of 2.5° taken half a sting chord in front of the nose of the model sting. This is clearly seen in Fig. 6. It is seen that the propeller slipstream puts the model sting locally at an angle of sideslip. This results in a slightly alternated local pressure distribution around the model sting. This is seen in Fig. 7. It is clearly seen in Fig. 7 that the pressure distribution at the sting changes locally near the fuselage. This results in a $\Delta\phi$ directly noticeable as a change in pressure projection on the fuselage. However clearly present, integrating this pressure change leads to a negligible net effect on both near-field as far-field effects.

A way to look at the power effects on the far-field disturbances is by studying the change in the spanwise distribution of the disturbance parameters $\Delta\alpha$ and $\frac{\Delta q}{q_\infty}$. For the power-on and power-off cases, these values are calculated. Subtracting the values of $\Delta\alpha$ and $\frac{\Delta q}{q_\infty}$ of the power-off case from the values as found for the power-on case leads to the engine power effects on these far-field parameters. But how are the values of $\Delta\alpha$ and $\frac{\Delta q}{q_\infty}$ determined? Consider the power-off cases. For both cases (including- and excluding the support), the wing section pressure distribution is calculated at various spanwise stations. Integrating these distributions leads to a spanwise distribution of the lift $c_l(y/b)$ for these cases (the spanwise coordinate y is non-dimensionalized by the wing span b). Subtracting these lift distributions then leads to the support influence on the local lift distribution. It can now be said that:

$$\Delta c_l(y/b) = c_{l_\alpha}(y/b)\Delta\alpha(y/b) + c_l\frac{\Delta q(y/b)}{q_\infty} \qquad (3)$$

In Equation 3 the local disturbance is related to a change in angle of attack and dynamic pressure resulting from the disturbance of the support. The local lift slope c_{l_α} is given the value 2π according to thin airfoil theory. For the local value of the lift-coefficient the undisturbed value is taken. For a number of spanwise stations, the value of $\frac{\Delta q(y/b)}{q_\infty}$ can be determined by subtracting the values of the static pressures in the airfoil stagnation points of both configurations

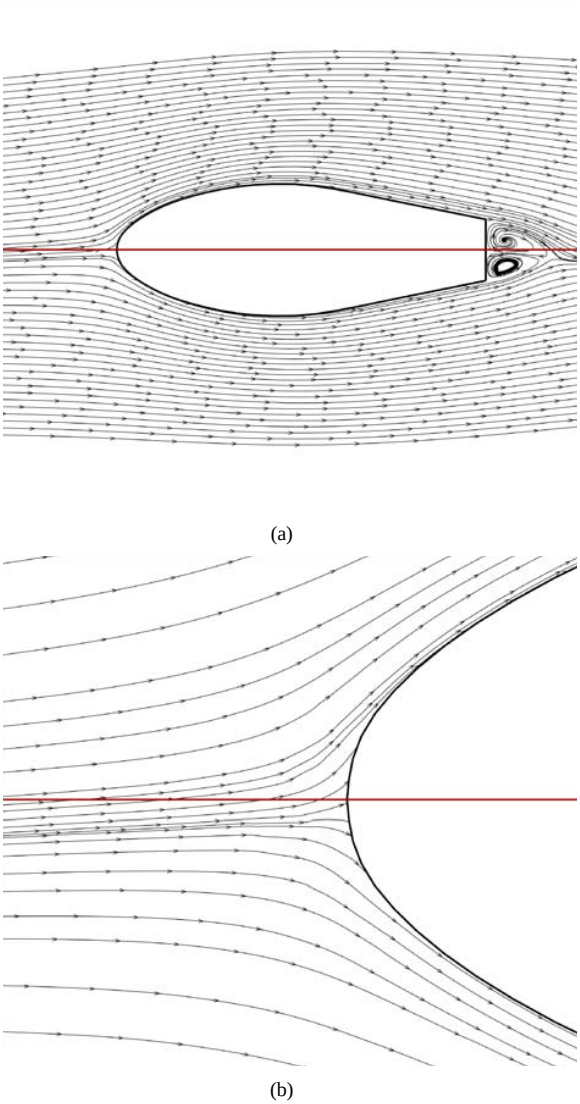

(a)

(b)

Fig. 6. Effect of the propeller slipstream on the local angle of sideslip at the model sting (a) A top view of a cross sectional plane of the model sting very close to the fuselage showing the local streamlines. As a reference the symmetry line of the sting is shown (b) The same as (a) but focused near the nose of the model sting

(including- and excluding the support). Applying the law of Bernoulli on the stagnation streamlines and assuming an equal total pressure in the undisturbed flowfield upstream of the configurations it is seen that the disturbance in dynamic pressure of the airfoil is related to this change in stagnation pressure. The stagnation points of the sections are the only usable points whereas at these points the flow is not affected by a change in angle of attack due to the action of the airfoil. When these values are known, the spanwise disturbances in angle of attack can be calculated using Equation 3. This same exercise is carried out for the power-on case. Subtracting the spanwise distributions of $\Delta\alpha$ and $\frac{\Delta q}{q_\infty}$ of the power-off case from the power-on case leads to the engine power effects on these far-field disturbance parameters. The results are given

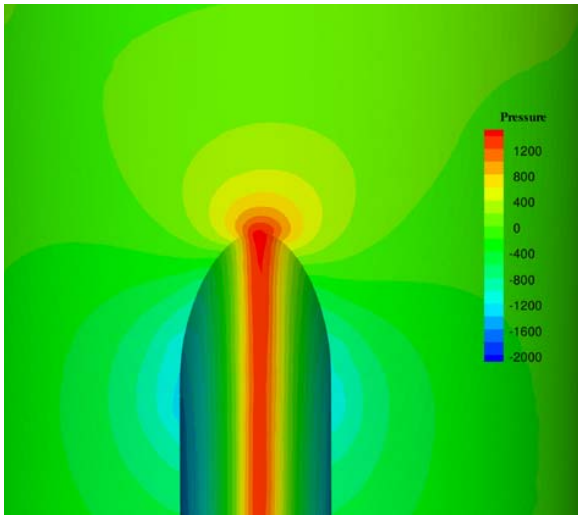

Fig. 7. Effect of the propeller slipstream on the local pressure distribution at the model sting and fuselage. The viewpoint is from upstream looking downstream at the leading edge of the sting at the bottom of the aircraft fuselage. Contours of relative pressure level ([Pa]) are plotted. The pressure is taken relative to a free-stream reference of 0 [Pa]

in Fig. 8.

It is seen in Fig. 8 that due to the change in disturbance potential caused by engine power effects, the local values of the disturbance in angle of attack and dynamic pressure are affected to quite some extend. For the disturbance $\Delta\alpha$ it is seen that changes of nearly 0.75° are found close to the fuselage. Because the local stagnation point on the sting near the fuselage shifts to the port side of the sting caused by the slipstream drift, the sting effectivity in increasing the angle of attack locally is reduced. This reduction is mostly noticeable at the starboard side where it is seen that the engine power effect reaches a maximum value. This causes the distribution of the engine power effects on the value of $\Delta\alpha$ to be asymmetric. Regarding Fig. 8(b), the distribution of the engine power effect on the disturbance in $\frac{\Delta q}{q_\infty}$ is also asymmetric. Looking at the pressure distribution in Fig. 7 this is to be expected. The local engine power effects on $\frac{\Delta q}{q_\infty}$ reach a maximum value at the starboard side of approximately -0.015. These negative values might originate from the fact that due to a local shift in stagnation location to the sting side, the flow locally sees a more blunt object causing the local dynamic pressure to decrease. In Fig. 8 it is seen that the engine power effects go to zero at the wing tips. Close to the fuselage, these effects are significant. When combined with the local aerodynamic properties of the wing however, the net engine power effects of the propellers are negligible for this configuration.

The conclusions that can be drawn from this are:

1) The displacement effect of the engine slipstream puts the model sting locally at an angle of sideslip different from the free-stream value. This is caused by the fact that two

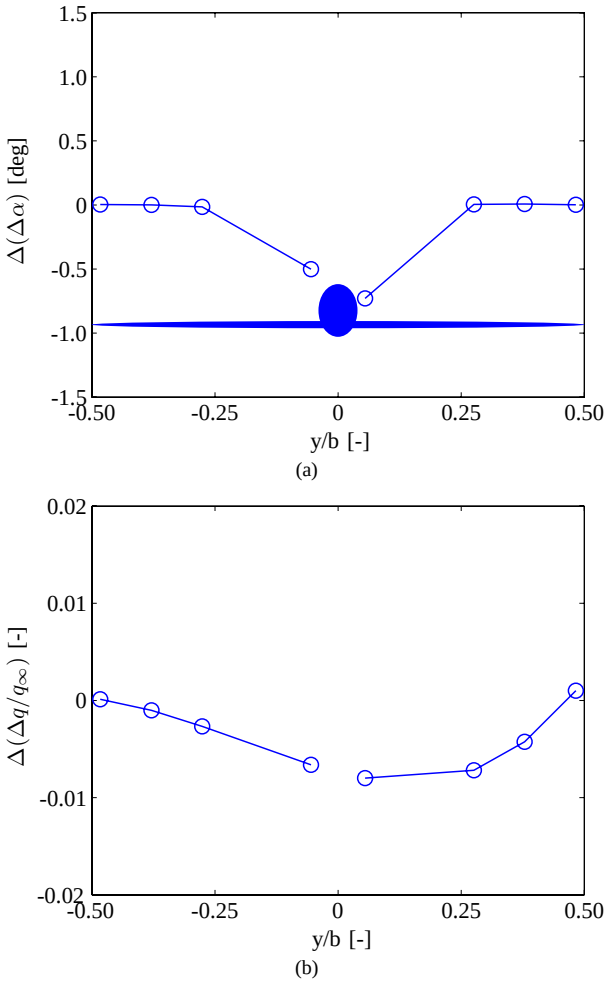

Fig. 8. The change in spanwise distribution of the disturbance parameters (a) $\Delta\alpha$ (b) $\frac{\Delta q}{q_\infty}$ due to engine power effects. The spanwise coordinate is non-dimensionalized using the wing span b

co-rotating propellers are discretized in the calculations. When contra-rotating propellers would be discretized the slipstream would induce a local change in angle of attack at the sting leading edge. Such changes are not thought to affect the model support near-field and far-field effects to a substantial amount

2) This local change in angle of sideslip induces a change in disturbance potential ϕ of the model sting
3) $\Delta\phi$ is noticeable studying the pressure distribution at the model sting
4) The engine power effect on the near-field disturbances are found as a change of sting pressure projection onto the fuselage. The net result of the engine power effects on the value of the near-field effects for this configuration is approximately zero
5) As a result of $\Delta\phi$ the far-field disturbances are also affected. The extend of the engine power effects on the local far-field disturbances is significant. Combined with the local aerodynamic properties of the wing these effects have a net negligible effect for this configuration

In these conclusions it is emphasized that these results count for the configuration under study. It is very well possible that when the configuration under study changes, the net engine power effects on the values of the near-field and far-field disturbances become significant. For example, when the configuration is set at an angle of sideslip such that the propeller slipstream interacts directly with the sting, the value of $\Delta\phi$ is very likely to increase substantially. Large local values of engine power effects on the near-field and far-field effects are expected. The magnitude of these effects is likely to depend on the placement of the sting with respect to the model and the local aerodynamic properties of the wing. Placing the sting in regions of adverse pressure gradients (e.g. at the backbody of the fuselage) increases the risk of considerable engine power effects on the near-field disturbances once the flow is unable to reattach on the fuselage aft of the model sting due to the slipstream effects. The local values of the far-field disturbances are also affected by this. Their net effect might become considerable when combined with local aerodynamic wing characteristics showing high values in the distribution of e.g. lift (due to the deflection of flaps for instance). In future experiments care should be taken in the setup of wind tunnel tests involving model engines. The magnitude of engine power effects on support disturbances can be decreased by ensuring that the engine slipstream maintains a maximum distance from the model support parts. Besides this, the sensitivity of the near-field and far-field disturbances to engine power effects must be minimized by choosing an appropriate placement of the support parts with respect to the wind tunnel model. This is realized by choosing a placement of the sting that is removed as far from the wing as possible while still attached to the cylindrical part of the fuselage.

IV. Conclusion

In this paper engine power effects on support disturbances are presented as secondary support disturbances because they can be seen as additional disturbances of the model support caused by a change in support disturbance potential ϕ. $\Delta\phi$ is caused by the slipstream of wind tunnel model engines. This slipstream induces a local change in angle of sideslip at the model sting thereby influencing the local sting near-field and far-field effects. Whether or not the total net result of these changes in the disturbance pattern leads to a significant engine power effect depends on the configuration of the wind tunnel model and the test setup. Experimental techniques demonstrating the determination and trends of these engine power effects are shown by discussing results of a measurement campaign performed by DNW on a four-engine turboprop aircraft. CFD results on a more generic model are presented in order to clarify the above mentioned mechanism behind engine power effects on support interference. Based on this information, recommendations can be given for future tests in order to minimize engine power effects on support interference. The magnitude of these effects can be decreased by ensuring that the engine slipstream maintains a maximum distance from the model support parts. Besides this, the sensitivity of the near-field and far-field disturbances to engine power effects must

be minimized by choosing an appropriate placement of the support parts with respect to the wind tunnel model. This is realized by choosing a placement of the sting that is removed as far from the wing as possible while still attached to the cylindrical part of the fuselage.

ACKNOWLEDGMENT

The authors wish to express their gratitude to the German-Dutch Wind Tunnels (DNW) for their support in providing data as presented in this paper and commenting on the paper content.

REFERENCES

[1] B.J.C. Horsten and L.L.M. Veldhuis, *Experimental and Numerical Results on Cavity Effects in Juncture Flow*. Conference Proceeding of the 38th Fluid Dynamics Conference and Exhibit, Seattle, Washington, United States, 2008.

[2] L.L.M. Veldhuis, *Support Interference Effects of a Ventral Sting on a Body of Revolution. A Brief Description of Phase 1*. Technical Report LSW 89-2, Delft University of Technology, Department of Aerospace Engineering, April 1988.

[3] D. Eckert, *Correction of Support Influences on Measurements with Sting Mounted Wind Tunnel Models*. AGARD FDP Conference, Brussels, Belgium, 1993.

[4] D. Eckert, H.G. Hegen and W. Kühn, *DNW's Method to Correct for Support and Wall Interference Effects on Low Speed Measurements With a Large Propeller Powered Transport Aircraft Model*. Conference Proceeding of the 25th International Congress of the Aeronautical Sciences, Hamburg, Germany, 2006.

[5] J.K. Nathman, *VSAERO, A Code for Calculating the Nonlinear Aerodynamic Characteristics of Arbitrary Configuration*. User Manual Version 7.0, Analytical Methods, Inc., 2003.

Bart J.C. Horsten B.J.C. Horsten (Bart) is a PhD. student at Delft University of Technology, Faculty of Aerospace Engineering, Aerodynamics Division. From 1999 to 2005 he was a college student at this faculty where he graduated in 2005 at the chair of Aerodynamics. During his graduation, he wrote a DNS code in order to perform laminar and turbulent simulations on riblet geometries. Aim of the research was to investigate the turbulent viscous drag reduction mechanisms caused by different riblet geometries implemented by the Immersed Boundary Method. After graduating at Delft University of Technology, a PhD. project was started in cooperation with DNW (German-Dutch Wind Tunnels) on the design of an Expert System for dealing with wind tunnel wall- and support interference. This is still his topic of research today.